


Microstructural, mechanical and fracture characterization of metal matrix composite manufactured by accumulative roll bonding 

Pereira G.S.¹, Da Silva E.P.², Requena G.C.^{3,4}, Avila J.A.⁵, Tarpani J.R.^{1,}*

1. Department of Materials Engineering, University of Sao Paulo (USP), Av. Joao Dagnone 1100, Jd. Sta Angelina, 13563-120, Sao Carlos, SP, Brazil.
2. Institute of Engineering, Science and Technology (IECT), Federal University of Vales do Jequitinhonha e Mucuri (UFVJM), 39447-790, Janauba, MG, Brazil.
3. Institute of Materials Research German Aerospace Centre, Cologne, Germany.
4. Metallic Structures and Materials Systems for Aerospace Engineering, RWTH Aachen University, 52062 Aachen, Germany.
5. Sao Paulo State University (UNESP), Campus of Sao Joao da Boa Vista, Av. Prof. Isette Correa Fontao, 505, Jardim das Flores, 13876-750, Sao Joao da Boa Vista, SP, Brazil.

*Corresponding author: jrpan@sc.usp.br

Research objective

To incorporate micro-silicon carbide particles in commercially pure aluminium 1100 by accumulative roll bonding process, and study microstructural changes and their effect on the mechanical properties and fracture mechanisms.

Research goals

- Manufacture micro-silicon carbide particles-reinforced metal matrix composite laminate via accumulative roll bonding by adopting affordable fabrication route.
- Microstructural characterization by scanning electron microscopy, energy dispersive X-ray spectroscopy, computed X-ray microtomography, backscattered electron diffraction and X-ray diffraction to determine potentially acting strengthening mechanisms.
- Mechanical characterization by hardness, notch tensile and ball-cratering wear tests to envision potential application field for the end-product.
- Fracture inspection to identify and characterize operating failure mechanisms as affected by the reinforcing particulate phase.

Highlights

Accumulative roll bonding process after 7 lamination passes reasonably dispersed micro-scale reinforcing particles in aluminium matrix.

1. Silicon carbide particles imparted hardness, and only moderately enhanced tensile properties of unnotched and notched specimens.
2. The metal matrix laminate was insensitive to geometrical stress raisers in terms of ultimate strength, stiffness, and toughness at maximum load.
3. The ceramic particulate granted outstanding wear resistance to the composite laminate by acting as effective solid lubricant.
4. Shear and dimple nucleation, growth and coalescence fracture mechanisms prevailed in tensile loading, while abrasion, adhesion and delamination mechanisms governed wear properties.

Abstract: Accumulative roll bonding is a severe plastic forming process recently proposed to manufacture ceramic particle reinforced-multi-layered metal matrix composites. In this work, low-cost composite multi-layered laminate was produced by roll bonding commercially pure aluminium 1100 with 5% in volume of reinforcing micro-scale silicon carbide particles. Microstructural features, hardness, tensile properties in the presence of stress concentrators, and wear resistance were assessed. Fracture surface inspection was carried out to determine operating failure mechanisms. Hardness was significantly enhanced, whereas tensile properties only moderately improved by ceramic particles incorporation. The main reasons were limited recrystallization and work-hardening relief due to periodic annealing, not completely dispersed particulate phase, some particle agglomeration. Though tensile properties increments were not much attractive, exceptional increase in wear performance was achieved due to the addition of ceramic particulate phase, which acted as solid lubricant mitigating abrasion, adhesion, and delamination wear mechanisms. The use of the manufactured composite laminate could then be worthwhile in applications where low-cost, notch insensitivity, and superior wear resistance are design requirements.

Keywords: A. Particle-reinforcement; B. Mechanical properties; D. Microstructural analysis; E. Forming.

1. Introduction

Ceramic particulate reinforcing-metal matrix composites (hereafter MMC) offer higher specific elastic modulus and ultimate strength (properties/weight ratios), better corrosion and wear resistance and greater thermal and dimensional stabilities than the base metal [1,2]. However, the expanded use of this composite material has been limited by its high manufacturing costs according to the routes currently available, such as powder metallurgy, casting, spray casting and positive and negative (vacuum) pressure infiltration. On the other hand, traditional technologies like strip and ingot casting followed by secondary mechanical processes present poor reinforcing-particles dispersion, high porosity levels and weak bonding between ceramic reinforcement and metal matrix leading to deficient mechanical properties [2,3,5].

To overcome these constraints, accumulative roll bonding (hereafter ARB) process, a genuinely continuous solid-state manufacturing route used to increase the mechanical performance of metal sheets via grain size refinement and strain-hardening mechanisms [6,7], has been proposed for obtaining low-cost, continuous large-scale production, increased strength and structurally refined multi-layered microparticulate-reinforced MMC composites [5]. Strictly speaking, ARB is a method of rolling a stack of metal sheets, which are repeatedly rolled to a severe reduction ratio under harsh shear and compressive loads, sectioned into two halves, piled again to be the initial dimension and rolled. Typically, less than 12 rolling passes have been employed by researchers to manufacture SiCp-reinforcing MMC via ARB. This technique can be easily adapted and integrated into existing continuous industrial rolling trains without major modifications and be scaled up to produce low-cost laminated materials with an ultra-

fine-grained microstructure [8]. ARB is not only a heavy-straining process but also a solid-state deformation bonding method, and large strains can be accumulated in the metallic laminate without any geometrical change in the worked piece. Redundant shear strain due to large friction during rolling can lead to ever-increasing through-the-thickness microstructure refinement and uniformity [9-11].

Improved particulate silicon carbide (hereinafter SiCp) dispersion, low porosity, imparted tensile and layer bond strengths have been reported in ARB-processed MMC comprising SiCp-reinforcing commercially pure aluminium (henceforth Al) from 1050 to 1100 grades [4,5,12]. Lower initial thickness, higher rolling speed and large rolling reduction have been determined as essential factors for improving bond strength. The effect of pre-, post-, and continuous rolling annealing on SiCp scattering, metal formability related to work-hardening recovery, recrystallization, interlayer diffusion and consolidation (bond strength) has also been investigated [13-16].

Lee et al. [17] found that variations in the ultimate tensile strength of Al-1100 base metal and the corresponding MMC with 5 vol.% SiCp simultaneously submitted to the ARB process was similar. However, due to higher matrix grain refinement in the MMC because of the presence of the ceramic particulate, the strength gain of the Al-SiCp composite was larger than the base metal. The same trend regarding grain refinement acceleration and efficacy due to ceramic particulate presence was observed by Alizadeh et al. [18] working with Al-1100 7 vol.% SiCp composite.

Regarding the reinforcing particle size effect, Jamaati et al. [19] cold worked Al-1050 with 10 vol.% SiCp and discovered that microstructural refinement evolution, reinforcing particle dispersion and low porosity tensile strength with larger (40 μm) particles was more remarkable and earlier attained than 2 μm particle size.

Wagih et al. [20] investigated ARB to produce Al-1050 4 vol.% SiCp composite and determined the main strengthening mechanisms as grain refinement, strain-hardening due to rolling process, while the addition of SiC nanoparticles acts as a secondary strengthening source.

Melaibari et al. [21] studied ARB to manufacture Al-1050 5 vol.% SiC composite and observed that warm accumulative roll bonding breaks reinforcing particles agglomerates thus improving their uniform dispersion throughout the metal matrix, and so hardness, strength, ductility, toughness and bond strength were imparted.

Fathy et al. [22] evaluated the mechanical properties of MMC comprising Al-1050 base metal and 1 to 4 vol.% reinforcing SiCp and emphasized the strong mechanical bonding taking place at the interface of the particle matrix, thus improving hardness, tensile strength and elongation, and determined the fracture mechanism was by shear ductile rupture.

Darmiani et al. [23] researched the wear resistance of Al-1050 containing 4 wt.% nanometric SiC particles and accredited the improved performance to increasing uniformity of ceramic particle distribution in the metal matrix, grain refinement and strain-hardening effects achieved during ARB cycles.

Potential strengthening mechanisms in SiCp-reinforced Al matrix ARB composites are: grain size refinement and well-developed high-angle grain boundaries causing dislocation pile-up, strain-hardening on the metal matrix, elastic and thermal mismatches, Orowan effect, back stress strengthening and work-hardening at the SiCp-Al boundary, besides load-transfer to the particulate phase. The operation, or not, of one or more mechanisms in a determined MMC laminate depends upon the lamination

processing parameters, the average particle size, particle size and dispersion, metal-ceramic interaction, detrimental phases, and porosity formation [13,24].

In the present work, an investigation is carried out regarding microstructural, mechanical and fractographical characterization of MMC comprising micro-SiCp dispersed in commercially pure Al-1100 by economical ARB route. The multi-layered MMC had as reference both the as-received Al-based foil and corresponding as-roll bonded laminate. Easily and rapidly fabricated, low-cost, notch insensitive MMC laminate, which can be employed in low-demanding applications where stringent wear performance is required, has been obtained.

2. Materials

Commercially pure Al-1100 grade (chemical composition in Table 1) received as 0.4 mm-thick cold rolled strips was utilized as the base-metal material. It typically exhibits good mechanical formability, excellent corrosion resistance, low cost, and wide availability. The as-received Al-1100 lamina was annealed at 350°C in N₂ atmosphere for 2 h to enhance their mechanical workability for subsequent ARB process.

Large average size (25 μm) low-cost commercial SiCp were employed as reinforcing phase due to their well-balanced properties, such as low density, high hardness and wear resistance, high thermal conductivity and thermal shock resistance and broad availability. SiCp were heat-treated at 900°C in air atmosphere for 2 h for surface decontamination and SiO₂ coating formation to improve compatibility and interaction with the metal matrix phase [4,5,13,22].

Table 1. Chemical composition (wt.%) of Al-1100 base metal.

Al	Si	Mn	Cu	Others
Balance	0.94	0.05	0.01	0.05

3. Experimental procedures

3.1 MMC manufacture

Four annealed Al-1100 strips with in-plane dimensions of 200 x 50 mm² were cleaned with organic solvent and brushed with steel bristles to remove the surface oxide layer and create roughness texture to induce metal/metal and metal/ceramic interaction. 2.5 vol.% of SiCp were then uniformly dispersed in appropriate amount onto the surface of three Al-1100 strips, which were then clamped by a steel wire along with the covering fourth strip to prevent their relative movement during the rolling process. Rolling direction was the same as the as-received Al-1100 strip.

Mechanical working progressed without lubrication in a double cold cylinder rolling mill with 13 tons radial load-capacity and rolls with diameter of 100 mm, whose speed was fixed at approximately 50 mm/min. A thickness reduction of 37.5% was imposed in the first lamination pass and 50% in the next six ones, for a total of just 7 passes, and the final laminate thickness was 1 mm. After each rolling cycle, the worked piece was cut in half and the two halves stacked together for a consecutive pass. SiCp were still added in the second and third cycles (1.25 vol.% per cycle) to obtain the targeted 5 vol.% SiCp-MMC laminate. The samples were heated in oven at 345°C for only 10

minutes before each rolling pass aiming at recovering work-hardening introduced in previous cold rolling cycle to enhance formability.

Identical procedures as above, except for SiCp addition, were applied to four annealed Al-1100 strips, and the strengthening role played by SiCp in the multi-layered MMC could therefore be identified.

To determine the effects of ARB process per se, the as-received 0.4-mm thick Al-1100 strip was also mechanically characterized and subjected to fractographic analysis.

All tensile tests were performed with the axial loading applied in the lamination direction.

Table 2 lists the variables of the ARB manufacturing process.

Table 2. ARB process variables.

Number of passes	Process temperature (°C)	Number of Al-1000 layers	Initial thickness of MMC per pass (mm)	Final thickness of MMC per pass (mm)	Thickness reduction per pass (%)
1	345	4	1.6	1	37.5
2	345	8	2	1	50
3	345	16	2	1	50
4	345	32	2	1	50
5	345	64	2	1	50
6	345	128	2	1	50
7	345	256	2	1	50

3.2 Microstructural analysis

Spatial SiCp distribution in the multilayered MMC, and degree of consolidation of both ARB products were evaluated by scanning electron microscopy (SEM) in FEI™ model Inspect F-50 operating in both secondary (SE) and backscattered (BSE) electron modes. It was equipped with Link Analytical™ Isis system for qualitative and quantitative elemental analysis (EDX). Computed X-ray microtomography (mCT) via RayScan™ model 250E complemented the SEM analysis.

Zeiss™ model Ultra 55 electron backscattering diffraction (EBDS) microscope and Panalytical™ X Pert PRO X-ray diffraction (XRD) equipment were utilized to identify possible phases transformation caused by ARB process, besides recrystallization, strain-hardening mechanisms, and crystallographic texture.

Samples preparation avoided deformation and the presence of oxides layers on the inspected surfaces. Manual wet grinding till 4000 mesh sandpaper and automated polishing with colloidal silica following 0.25 µm diamond paste were employed.

3.3 Mechanical properties

Zwick-Roell™ ZHVµ micro Vickers hardness tester was used to determine potential strengthening mechanisms operating during ARB process per se, and due to SiCp incorporation. Five measurements were performed in each sample, and average and standard-deviation values were obtained.

Monotonic tensile tests were carried out with cold rolled Al-1100 foil (baseline condition), Al-1100 and Al-SiCp MMC ARB laminates. Small-scale full-thickness

specimens with length and width of, respectively, 120 and 12.7 mm were tested according to the ASTM E8M standard. Unnotched and notched test pieces, presented in Fig.1, were studied.

Tests were conducted at room temperature in specimens with the longitudinal axis parallel to the rolling direction; EMICTM universal tensile test machine equipped with 5 kN load-capacity cell and operating under displacement control at strain rate of 2 mm/min was used. Strain was monitored throughout the test by an extensometer with initial gouge length of 25 mm. Tests were repeated three times for each material and specimen conditions up to complete rupture of the test coupons. Engineering stress-strain curves (load divided by gross section of the specimen) were plotted and average and standard-deviation values of typical mechanical properties like ultimate tensile strength and ductility (strain at fracture) were determined.

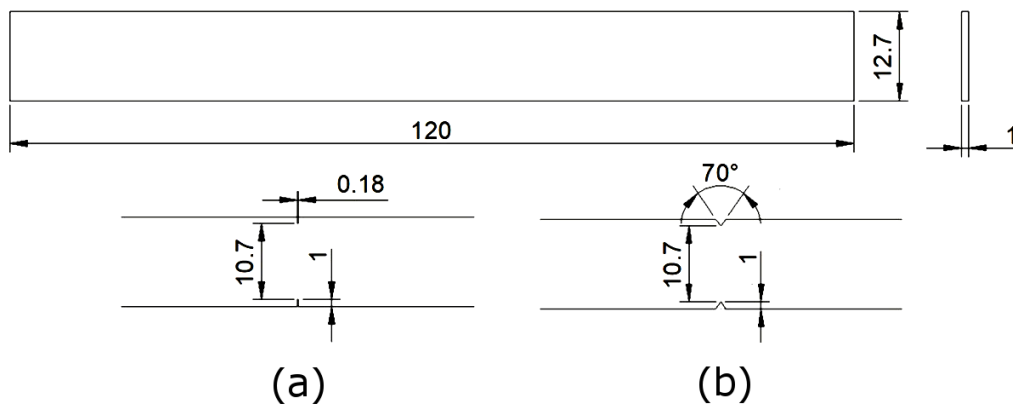


Figure 1. Notch geometries and dimensions in tensile test specimens: (a) slit (curvature radius of 0.075 mm), (b) V-notch (0.125 mm).

Ball-cratering wear tests were performed under dry conditions on fixed sphere equipment. SAE 52100 steel sphere with 25.4 mm in diameter travelling at 300 rpm and contacting the sample under 0.66 N load was utilized. Samples surface preparation

included progressively grinding till 2000 mesh sandpaper and cleaning in ultrasonic bath with acetone after each step. At the travelled distances of, respectively, 120, 239, 478 and 957 m (i.e., time travels 5, 10, 20 and 40 min) the spherical worn calottes were cleaned and photographed with Carl Zeiss™ model Axio Lab.A1 optical microscope for subsequent diameter measurement and removed volume calculation [25]. FEI-SEM™ model XL50 operating in secondary electron mode was used to characterize the morphological aspects of worn surfaces.

4. Results and discussion

4.1 Microstructural analysis

4.1.1 Scanning electron microscopy (SEM)

Figure 2 shows SEM images of cross-sectioned Al-1100 strip and Al-1100 MMC ARB laminates. Figure 2(a) shows practically inclusion-free Al-1100 ARB laminate, while Fig. 2(b) reveals the presence of few small pores. The homogeneous texture of the laminate is confirmed insofar as the interfaces of the multi-layered structure cannot be easily identified even under high magnification.

Figures 2(c-e) refer to the Al-SiCp MMC laminate after four accumulated rolling steps, where a relatively poor SiCp dispersion is noticed in Fig.2(c) as aligned ceramic particulate aggregation mainly located at the multilayer interfaces. Figure 2(d) presents a large pore created when a SiCp agglomerate was pulled out during the metallographic preparation. Fig.2(e) displays a large SiC particle, along with smaller ones surrounded

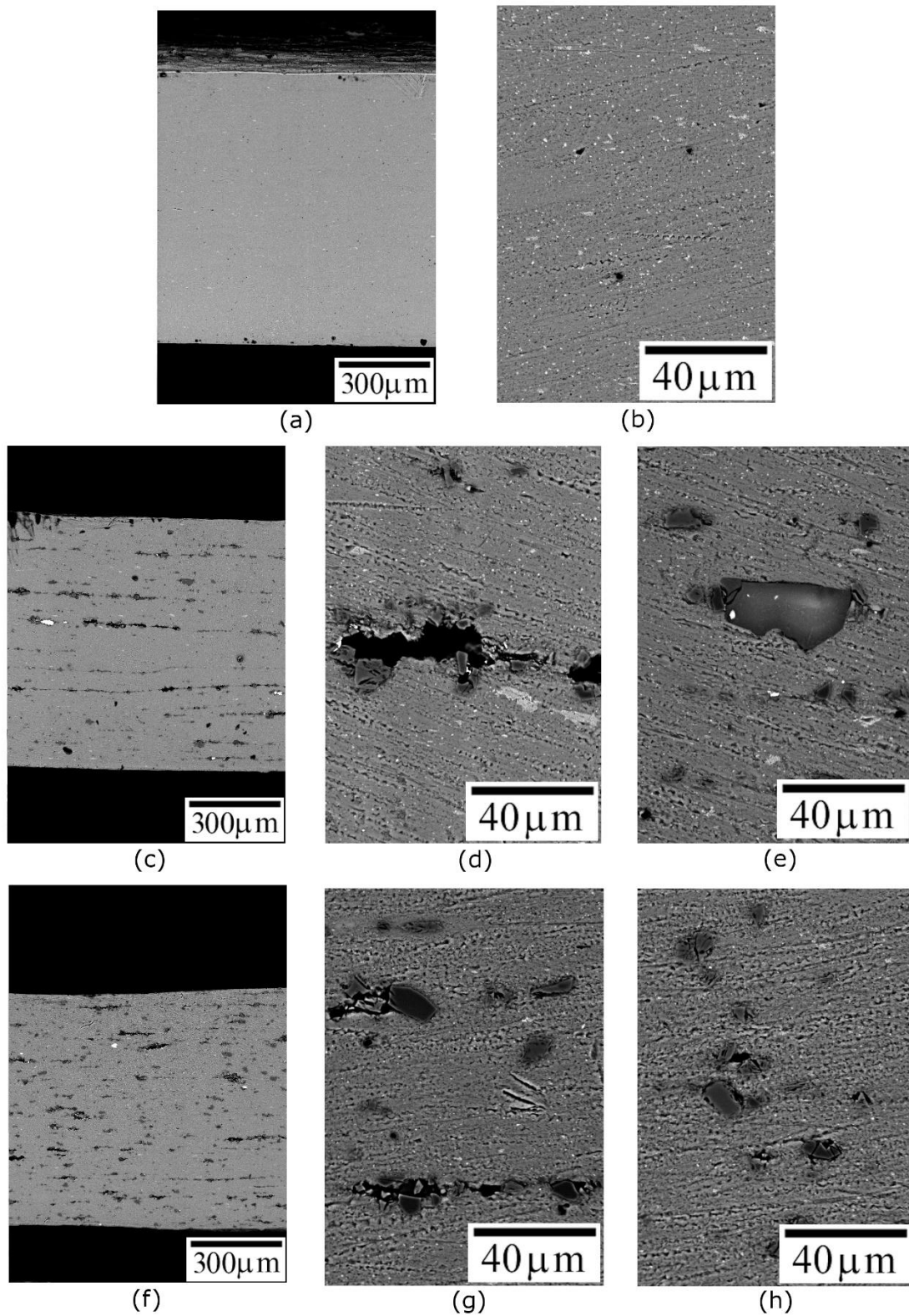


Figure 2. (a) Low and (b) high magnification SEM images (SE mode) of Al-1100 ARB laminate; (c,d,e) general and magnified views of MMC laminate after four rolling passes and (f,g,h) after seven rolling passes (BSE mode). The laminate thickness corresponds to the page height, and the lamination direction to the page width.

by the ductile matrix, indicating proper physical interaction between the phases.

However, an intermediate size particle at the bottom of the figure does not exhibit that desirable feature.

Figures 2(f-h) refers to the multi-layered MMC laminate after seven ARB passes, i.e., end-product. Segmented lines of agglomerated SiCp are noticed in Fig.2(f), indicating increased SiCp homogenization in the metal matrix due to additional lamination passes.

Figure 2(g) presents much smaller defects than observed in Fig.2(d), thus confirming less critical SiCp agglomerates in the latter case. SiC particle breakage and debonding can be observed in Fig.2(h). Considering that, to obtain a cost-effective end-product was intended, only a few rolling passes were employed in this study, the degree of consolidation can be considered satisfactory, i.e., relatively low porosity levels were achieved.

4.1.2 Energy dispersive X-ray spectroscopy (EDX)

Figure 3 shows EDX maps of cross-sectioned MMC laminate (same views as Fig.2).

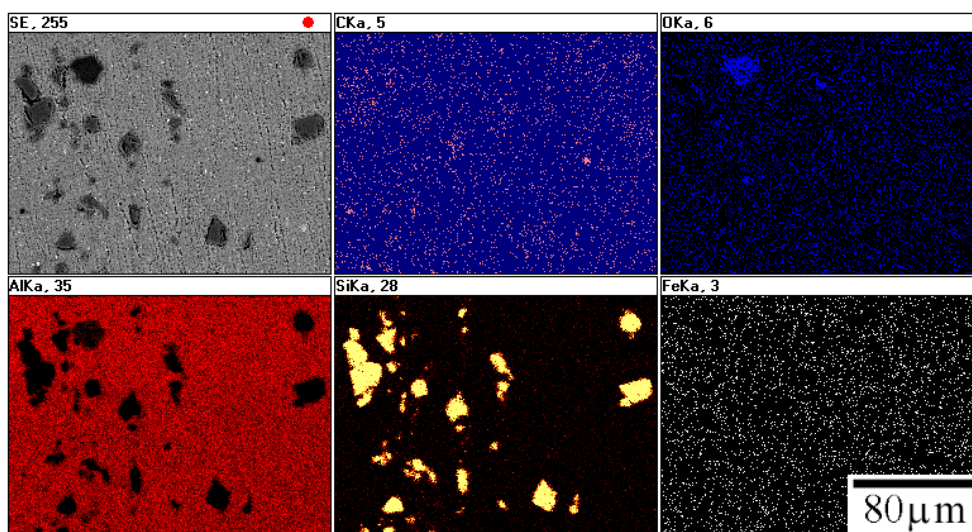


Figure 3. Chemical mapping of MMC laminate. MMC lamination direction corresponds to the page height and laminate width to the page width.

Small amounts of iron and carbon evenly distributed through the MMC bulk resulted from contamination by lamination rollers. Fairly good local dispersion of SiC particles and presence of oxygen-formed inclusions are revealed. There is no indication of extraneous phases formed during the ARB process.

4.1.3 Computed X-ray microtomography (mCT)

The reinforcing SiCp phase was analysed through mCT in Skyscan™1272 high-resolution 3D X-ray microscopy, and the results are presented in Fig.4.

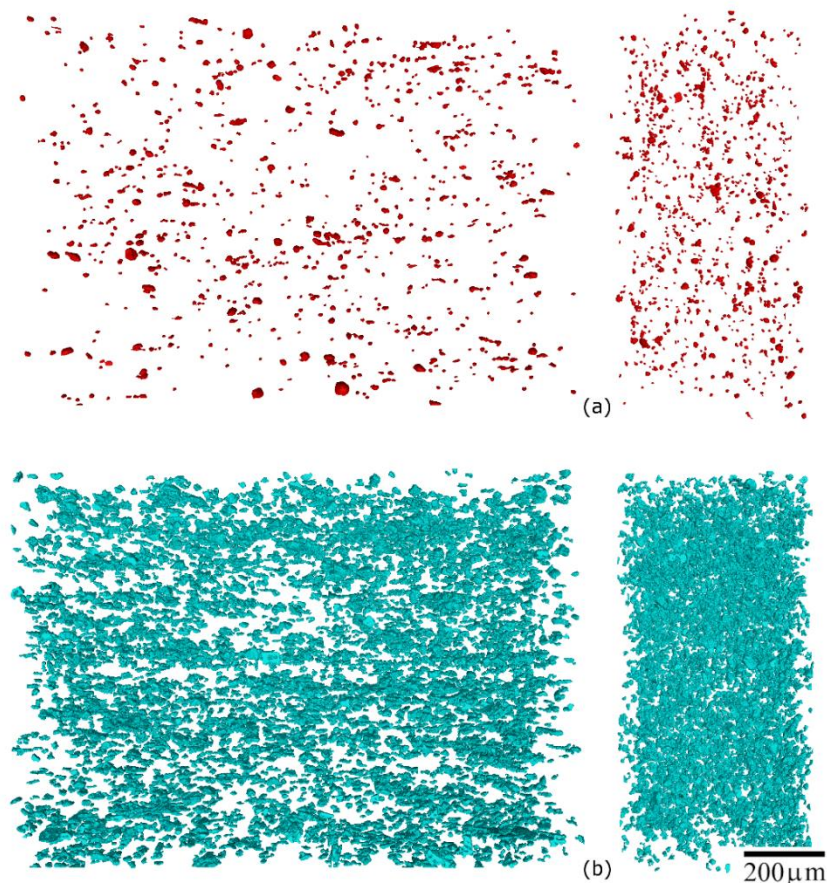


Figure 4. SiCp distribution maps from X-ray microtomography analysis. At left, MMC lamination direction corresponds to the page width; at right, the laminate width coincides with the page width. The image height refers to the laminate thickness.

The spatial distribution of denser particles is shown in Fig.4(a), while lighter carbide fragments can be seen in Fig.4(b).

A large particle size distribution, and good particle dispersion throughout the metal matrix can be confirmed regardless the particle density, thus corroborating Fig.2.

4.1.4 Electron backscattering diffraction (EBDS)

Figure 5 shows the EBDS inverse pole figure of Al-1100 ARB laminate, where colours are indexed to specific crystal orientations. Interlayer bonding failure is black coloured, indicating no crystallographic indexation.

Very deformed and elongated grains (high-angle boundaries) in the lamination direction are observed, with some subgrains (low-angle boundaries) within them. There is no evidence of recrystallization, indicating that the recrystallization temperature was not attained in the last annealing treatment (penultimate ARB pass).

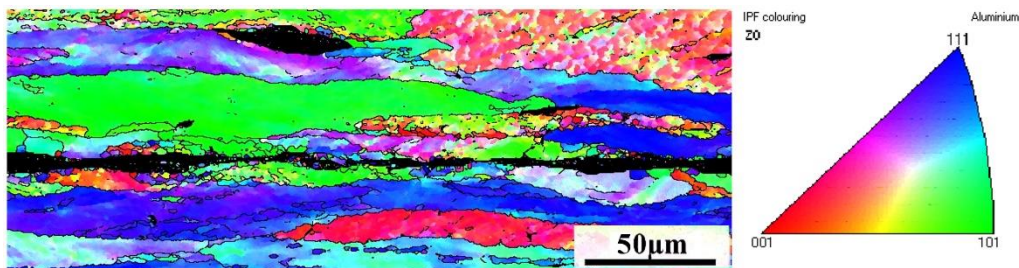


Figure 5. Inverse pole figure map of Al-1100 ARB laminate. The laminate thickness corresponds to the page height, and the lamination direction to the page width.

Figure 6 presents the inverse pole figure of MMC laminate, where only the Al phase was indexed in search for work-hardening and recrystallization signs. Delaminations and SiC particles are in black colour, meaning no crystallographic indexation. Grains

were less deformed than the Al-1100 ARB laminate (Fig.5). Previous researches [2,13,18] report that when the SiCp-reinforced MMC is exposed to severe plastic deformation, highly localized stress develops in the vicinity of non-deformable ceramic particles, which form barriers that inhibit the elongation of the metallic grain.

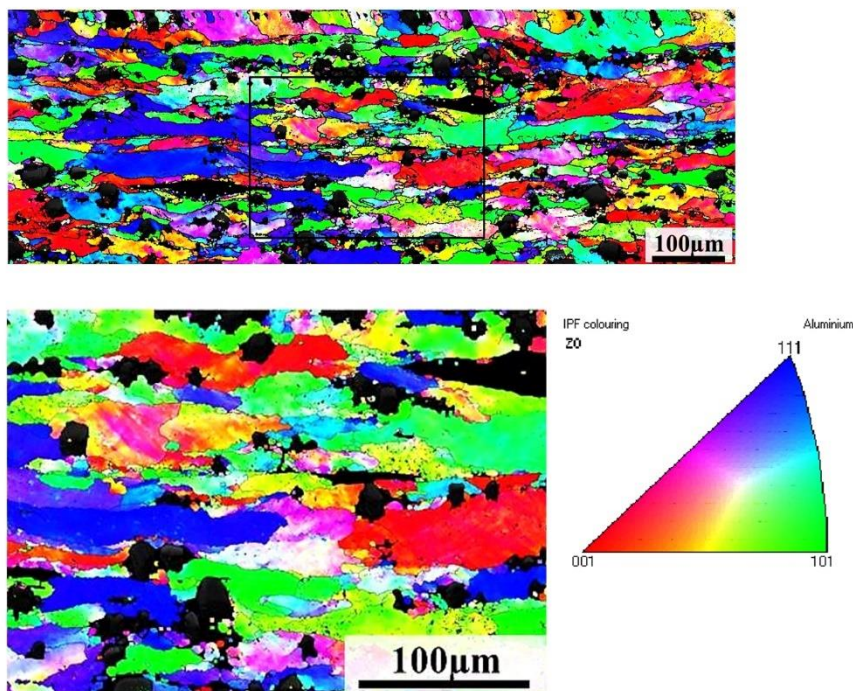


Figure 6. (a) Inverse pole figure map of the MMC laminate, (b) magnified view of the black rectangle area. The laminate thickness corresponds to the page height, and the lamination direction to the page width.

According to those authors, this morphology modification may induce nucleation of substrate grains by introducing high dislocation density. This “particle stimulated recrystallization process” seems not have been effectively triggered in the present case, indicating that accumulated work-hardening till the penultimate rolling pass did not provide activation energy enough to recrystallization. This signifies that pre-heating (345C° for 10 minutes) before each ARB cycle was effective in recovering metal

formability [26-28]. In addition, large SiCp average size much probably did not introduce enough dislocation density to induce grain refinement [29-31].

Oliveira et al. [32] observed finely dispersed precipitates in as-received Al-1100 sheets preventing recrystallization by restraining sub-boundaries movement. Recrystallization only occurred above 400°C following cold rolling to 80% area reduction. This indicates that the same mechanism must also have contributed to inhibited recrystallization in the present study, since area reduction on rolling passes was 50%, and subsequent annealing was carried out at 345°C.

Figure 7(a) shows the same MMC microstructure as in Fig.6, where metal matrix and ceramic particles are portrayed in red and blue colours, respectively.

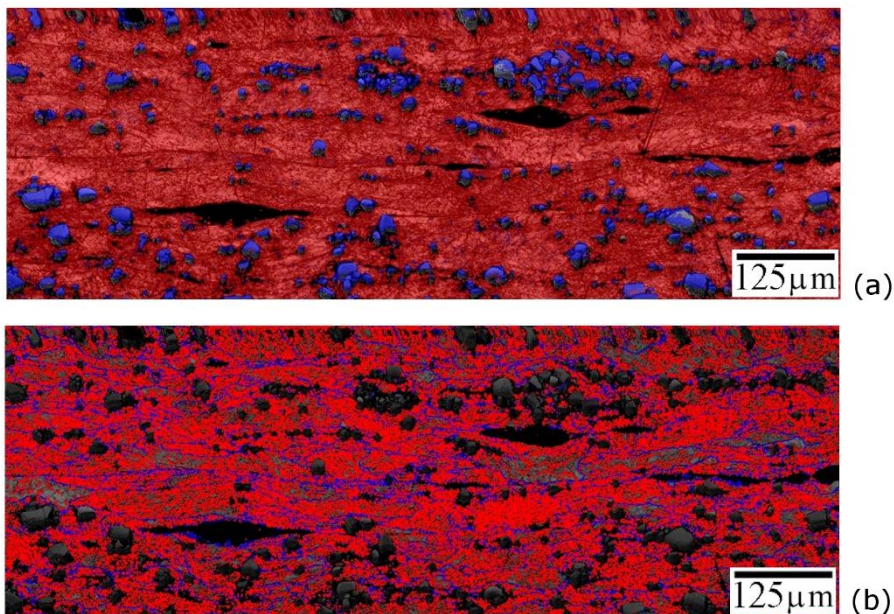


Figure 7. (a) MMC microstructure featuring metal matrix (red) and SiC particles (blue); (b) recrystallization map (highlighted in blue). The laminate thickness corresponds to the page height, and the lamination direction to the page width.

One can observe only moderate distribution of SiC particles in the metal bulk, as well as their trend to align as agglomerates in the interlayer planes, as previously revealed

by Fig.2. On the other hand, Fig.7(b) highlights tiny discrete recrystallized regions in blue, as originated by subgrain rotation [33], thus confirming the microstructural features shown in Figs.5 and 6.

Qualitative and quantitative analyses of acting strengthening mechanisms in the matrix phase of the composite are presented in Fig.8.

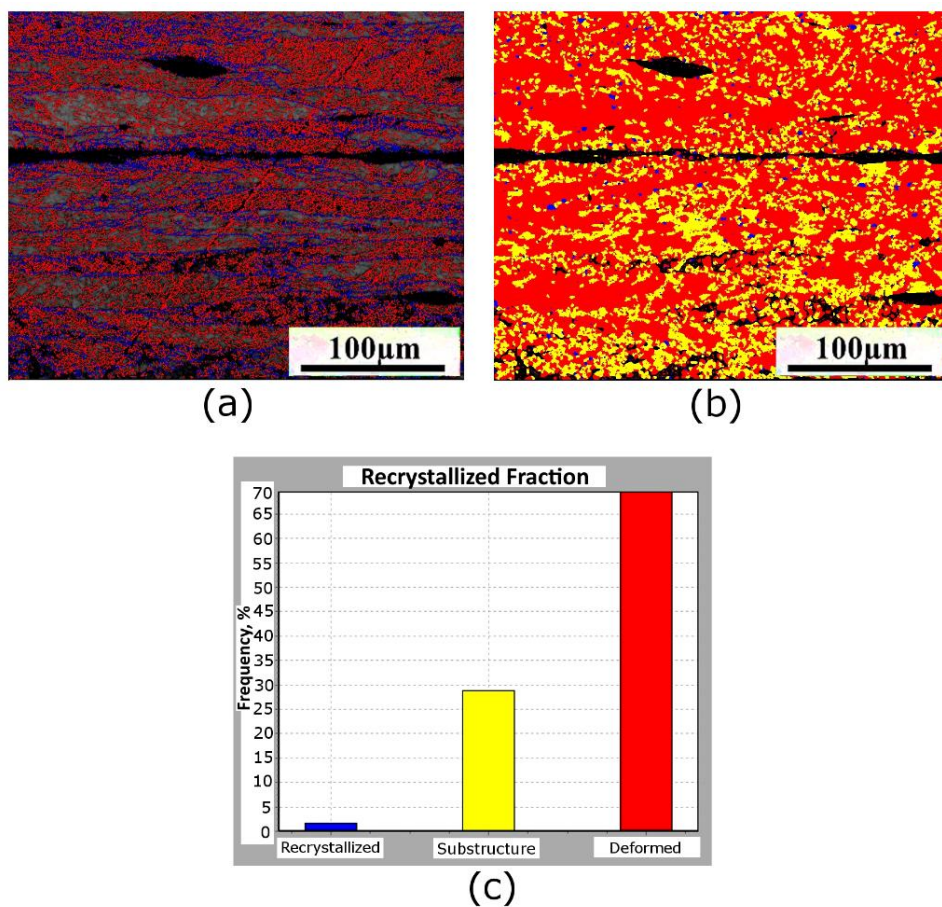


Figure 8. (a) Recrystallization, and (b) low and high-angle grain maps; (c) corresponding percentage area-based histogram. The laminate thickness corresponds to the page height, and the lamination direction to the page width.

Figure 8(a) shows small and sparse recrystallized regions in blue colour, whereas Fig.8(b) differentiates red coloured high-angle pancaked grains boundaries, above 15°, from less deformed low-angle yellow subgrains, between 2-15°. In situ observation [34]

indicates that low and particularly high-angle grain boundaries prevent dislocation glide across them, with the main sources of the impediment possessing geometrical and local structural stabilization natures.

Figure 8(c) provides the areal frequency distribution histogram of the above described mechanisms, permitting one to infer their magnitude in strengthening the MMC laminate.

Figure 9 shows stereographic projections for the Al-SiCp composite according to three different crystallographic orientations, as obtained by EBSD. The pole figures refer to the plate rolled surface.

Preferential crystallographic orientations of grains (rolling texture) with a maximum intensity of 3.57x is noticed. The strain-hardened structure in the lamination direction (corresponding to page width) derives from plastic deformation according to preferential crystallographic slip planes. The highest intensity (3.57x) is observed for the densest CFC lattice plane family $\{100\}$ (i.e., rotated cube texture), with deformation texture developing with the cube surface almost parallel to the plate surface, which is characteristic of cold rolling [35].

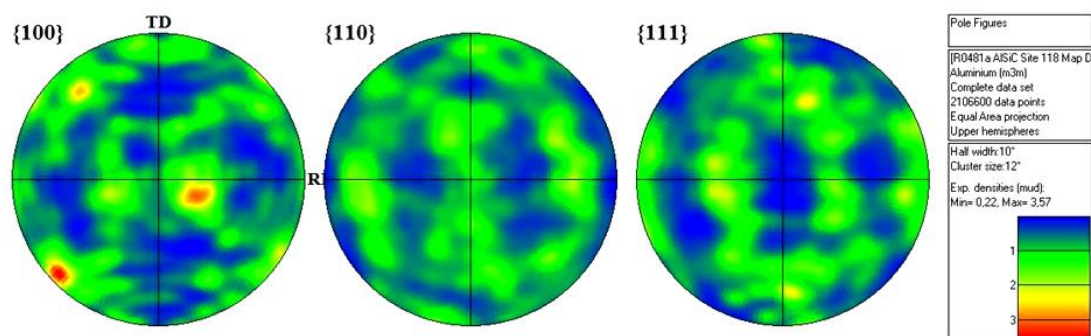


Figure 9. Stereographic projections for the Al-SiCp MMC. The rolling direction corresponds to the page width, and the plate width to the page height.

4.1.5 X-ray diffraction (XRD)

Figure 10 shows X-ray diffractograms obtained for both Al-1100 ARB and Al-SiCp MMC samples. Regarding the former laminate, only peaks belonging to the Al-alloy are present, while extra peaks related to the MMC laminate correspond SiCp. It can be concluded that no extraneous phases, which could impair the end-product performance, have been created during the manufacturing process. These results agree with those previously presented for EDX analysis and emphasize the advantages of solid-state fabrication process over other manufacturing techniques [2].

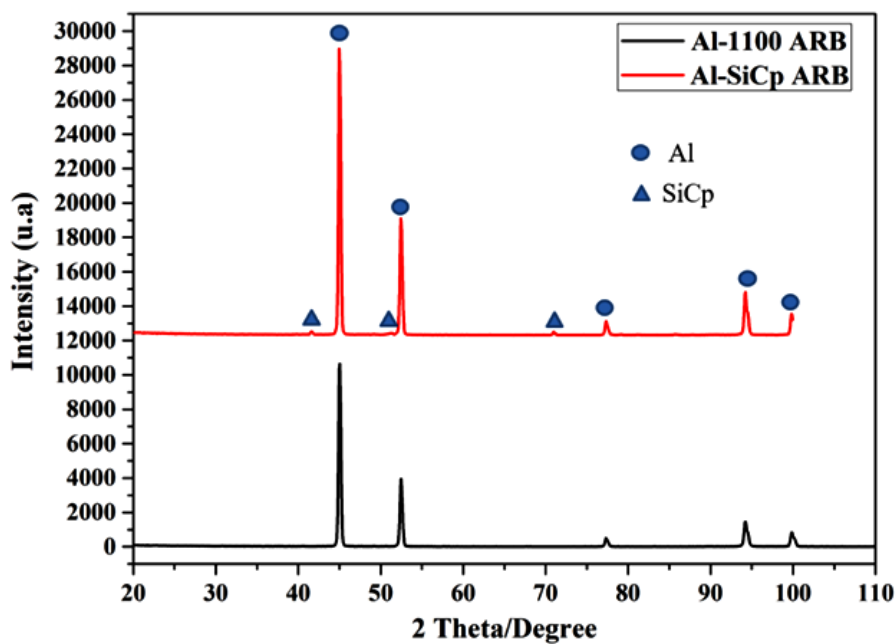


Figure 10. X-ray diffractograms of, respectively, Al-1100 and Al-SiCp ARB laminates.

4.2 Mechanical properties

4.2.1 Vickers hardness

Table 3 provides five hardness measurements, average and standard-deviation values for both the accumulative roll bonded laminates.

Table 3. Hardness testing results for the Al-alloy and the MMC ARB laminates.

Al-1100 ARB	AlSiCp MMC ARB
45.0	68.0
45.4	67.0
44.8	70.7
44.9	66.6
45.4	66.2
45.1 (0.3)	67.7 (1.3)

The Al-1100 laminate's hardness is much lower than reported by Santos-Filho [26] for the same material after annealing at 200°C, which was nearly 55 HV. According to those authors, grain refinement along with only partial work-hardening recovery during the heat treatment led to high hardness material. Considering that in the present work annealing was performed at substantially higher temperature (345 C°), and that recrystallization has practically not been developed in the end-product, lower hardness values can be considered consistent. Table 3 also confirms that the ARB-MMC laminate is significantly harder than ARB-laminate, because of SiCp incorporation.

4.2.2 Monotonic notch tensile testing

Average and standard-deviation values of ultimate tensile strength, and strain at rupture are listed in Table 4. The engineering stress-strain curves for all materials and specimen geometries tested are shown in Figs.11 and 12.

Table 4. Tensile testing results for all materials and three specimen geometries tested.

Material/Geometry	Ultimate tensile strength (MPa)		Strain at rupture (%)	
	Mean	SD	Mean	SD
Al-1100 unnotched	119	2.7	2.3	0.3
Al-1100 ARB unnotched	122	2.6	5.5	0.4
Al-SiCp ARB unnotched	133	3.1	6.3	0.3
Al-1100 slit-notch	67	1.6	6.5	0.2
Al-1100 ARB slit-notch	108	1.9	2.2	0.7
Al-SiCp ARB slit-notch	128	1.9	1.5	0.1
Al-1100 V-notch	65	1.4	6.3	0.9
Al-1100 ARB V-notch	119	1.8	3.3	0.2
Al-SiCp ARB V-notch	126	1.7	1.8	0.1

The high ultimate strength of as-received unnotched Al-1100 strip in Fig.11(a) indicates that severe work-hardening was attained during cold rolling [14,22,36,37]. Figure 11(b) shows that, in general, the Al-1100 ARB laminate approached well the as-received Al-1100 strip in terms of mechanical strength. Considering that the latter material was annealed before each of the 7 lamination passes, thus relieving previously imposed strain-hardening, other reinforcing mechanisms must have also developed. According to the literature [38-41], lamination processing induces extra strain-hardening at the contacting surfaces of two adjacent laminae (interface-affected-zone). In turn, back stress strengthening, and back stress work-hardening established at the strain-hardened interfaces confine dislocation motion within the layers, and powerful reinforcing mechanism are activated in the whole laminate. Outstanding laminate toughening due to pre-delamination effect has also been reported under such circumstances [38-40], whereby cracks nucleate in every formed interface-affected-zone, leading to high energy consumption during crack propagation caused by in-plane

shear stresses. This toughening effect can be confirmed by comparing stress-strain curves of unnotched specimens in Figs.11(a-c), where exceptional ductility of ARB-products contrasts with the restricted elongation of the as-received Al-1100 sheet.

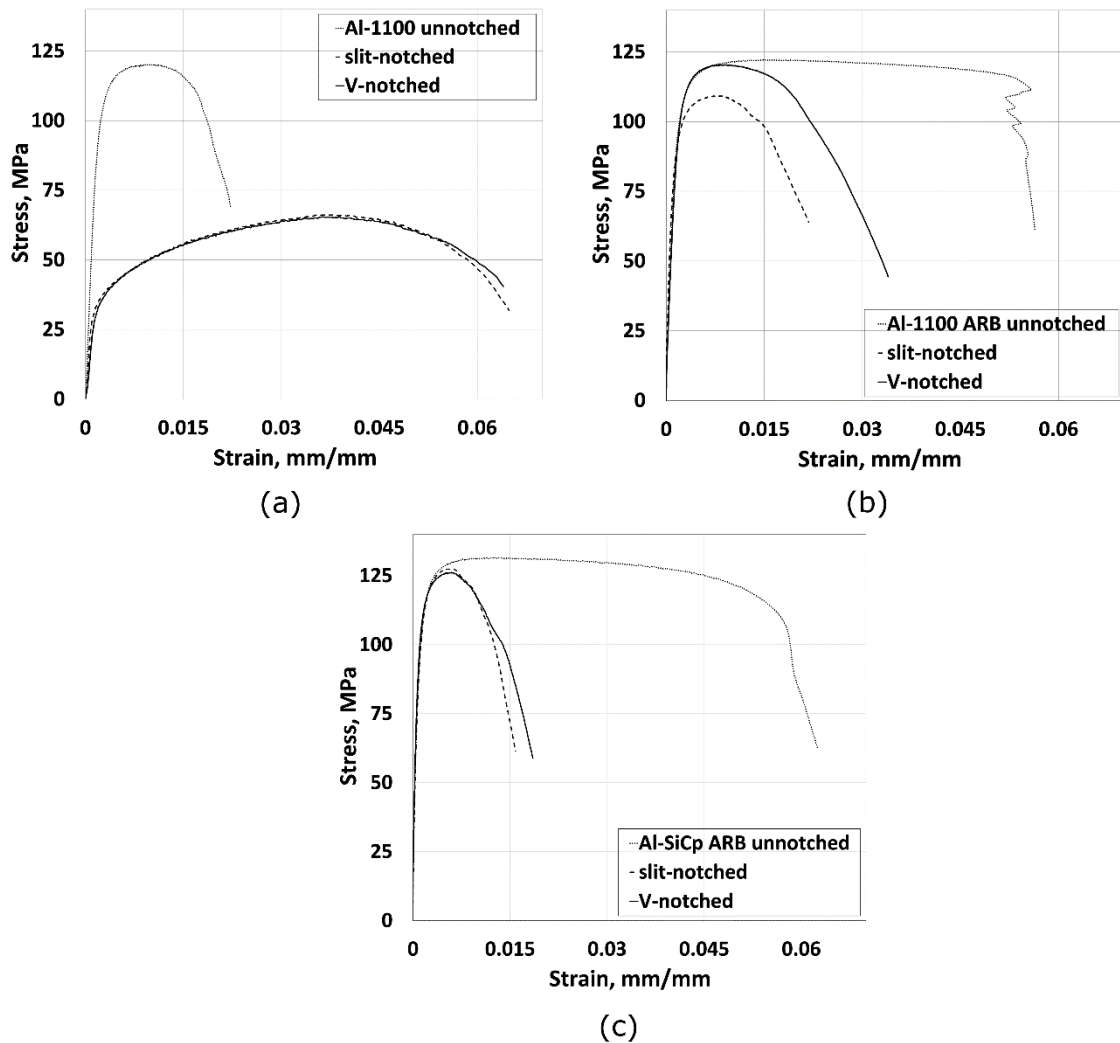


Figure 11. Engineering stress-strain curves for the three tested materials according to the specimen geometry.

Figure 11(a) also shows that the Al-1100 lamina is highly notch-sensitive, and the material weakens in the presence of geometrical discontinuities. This behaviour is caused by larger plastic zone ahead the notch tip, thus resulting in stress relaxation

[42]. According to Fig.11(b), the Al-1100 ARB laminate is sensitive to slit-notches, which are sharper than the V-notches, but in a much less extent than the Al-1100 sheet. Differently from the as-received Al-1100 lamina, strain at fracture (ductility) decreases in the Al-1100 ARB laminate when stress concentrators were introduced. The multi-layered nature of ARB structure facilitates delamination that absorbs energy at the expenses of plastic zone growth at the notch-tip (notch-induced embrittlement), granting the ARB laminate more fracture-prone.

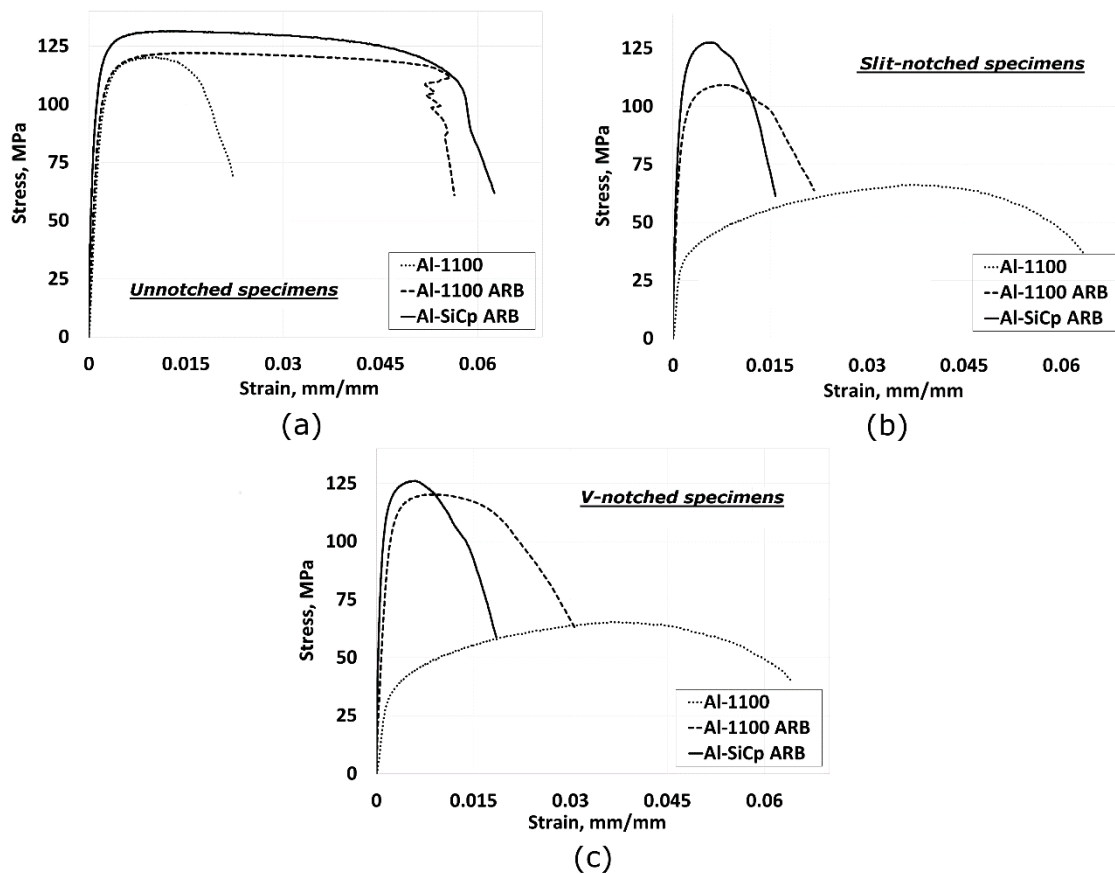


Figure 12. Engineering stress-strain curves for the three specimen geometries according to the material tested.

The same mechanisms acted as well in the notched Al-SiCp multi-layered MMC laminate. However, due to the presence of fragile SiC particulate, brittle behaviour is

enhanced and the material becomes practically notch-insensitive in terms of ultimate strength, stiffness, and toughness till the maximum load-carrying capacity. Since that intentional, and non-intentional discontinuities are inevitable in mechanical designs, presenting a variety of geometries and root radii, the advantage of the roll bonded MMC over its rivals becomes evident.

Figure 12 displays the same stress-strain curves provided in Fig.11, though it combines them differently to permit an alternative way to compare the mechanical performance of the materials tested. For instance, the MMC supremacy regarding all the tensile properties is noticeable.

Figure 13 portrays the tensile fracture surfaces created in the materials tested in different specimen geometries.

Figures 13(a-c), corresponding to the Al-1100 sheet, reveals ductile fracture typical of aluminium and its alloys, with microcavities nucleation, growth and coalescence occurring in the mid-thickness of all specimen geometries [15,22,24], where plane-strain condition prevails. Conversely, regions next to the specimen surface deform by pure shear (plain-stress condition). Notched specimens (Figs.13b,c) present a pronounced striation-like shear pattern (top and bottom of images) indicating that stress concentrators favour plastic deformation, thus confirming results provided in Fig11(a). The fully ductile fracture of Al-1100 ARB laminate in the unnotched condition is observed in Fig.13(d), thus complying with the respective stress-strain curve in Fig.11(b). On the other hand, notched specimens (Figs.13e,f) display somewhat brittle fracture aspects in the form of delaminations. The slit-notched specimen exhibits higher concentration of delamination sites than the V-notched one, though the latter condition depicts longer delaminations. Since stress-strain curves in Fig.11(b) indicate the slit-

notch as the most severe condition in terms of mechanical performance, potential delamination sites should then be avoided in this material, e.g., by minimizing SiCp clusters.

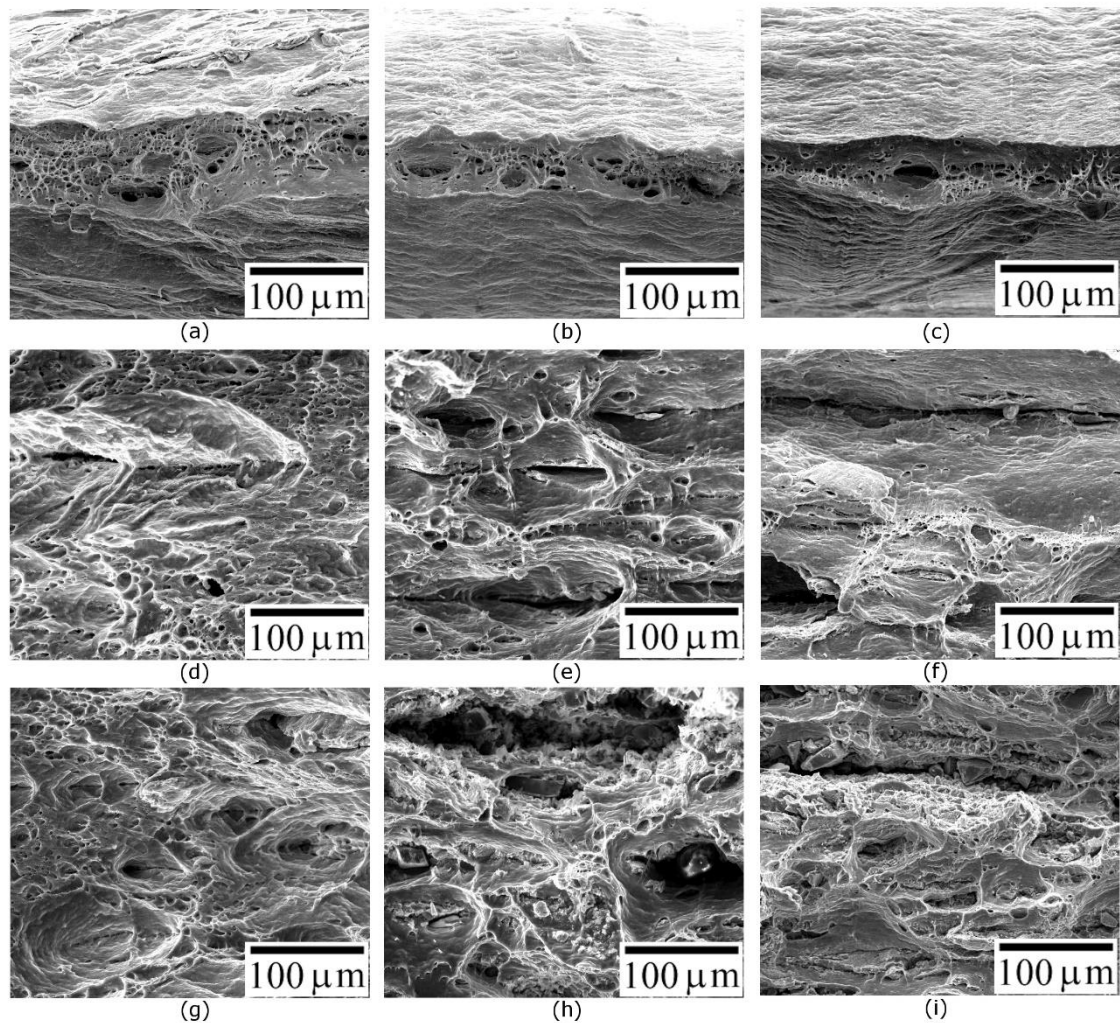


Figure 13. SEM images (SE mode) of tensile fracture surfaces: (a-c) as-received Al-1100 in unnotched, slit-notched and V-notched conditions, respectively; (d-f) the same sequence for Al-1100 ARB laminate; (g-i) the same for SiCp-Al1100 MMC ARB laminate. Rolling direction and laminate thickness are parallel to, respectively, the page width and height. All images with the same magnification.

Fully ductile fracture is also noticed in Fig.13(g) for unnotched MMC specimen, which agrees with stress-strain data in Fig.11(c). Figures 13(h,i) do not reveal any marked

difference in fracture aspect of slit and V-notched specimens, which agrees with the almost identical behaviour exhibited by the composite laminate when notched in one and other condition.

Despite the best overall tensile performance presented by the ARB-MMC laminate, it did not attained values of similar materials reported in the literature [2,4,5,12-24,26-28,36,37,44,45], though it approached well some reported results related to warm-laminated ARB composites [15,22]. In this regard, limited grain refinement, only moderately accumulated strain-hardening, modest SiC_p agglomeration breakage, and moderate particulate dispersion [5,16,24] may have compromise the tensile behaviour of the MMC laminate.

4.2.3 Wear testing

Table 5 shows the mean diameter values of the worn calottes in the Al-1100 and Al-SiC_p MMC ARB laminates, as obtained by optical microscopy (OM) measurements for different wear test stages.

Table 5. Wear testing results for the ARB laminates.

Time (min)	Calotte diameter Al-1100 ARB		Calotte diameter Al-SiC _p MMC ARB		Travelled distance (m)
	Mean (mm)	SD	Mean (mm)	SD	
5	1.77	0.04	0.67	0.13	120
10	2.08	0.01	0.77	0.02	239
20	2.46	0.02	0.80	0.17	478
40	2.95	0.08	1.02	0.15	957

Figure 14 shows wear resistance curves, where it is evident the successful incorporation SiC particles by increasing the wear performance (volumetric loss criterion) of the Al-1100 ARB laminate by almost two orders of magnitude. This result is quite significant, even though there is no data available in the literature regarding similar wear test performed in Al-SiCp ARB laminates. In fact, the only one wear test result refers to pin-on-flat experiments carried out by Darmiani et al. [23], who reported mass loss reduction by only half due to SiCp-nanoparticles incorporation at 4 wt.%. Considering that substantially more expensive raw-material and manufacturing process were utilized by those authors, the wear resistance gain in the present work can be considered remarkable

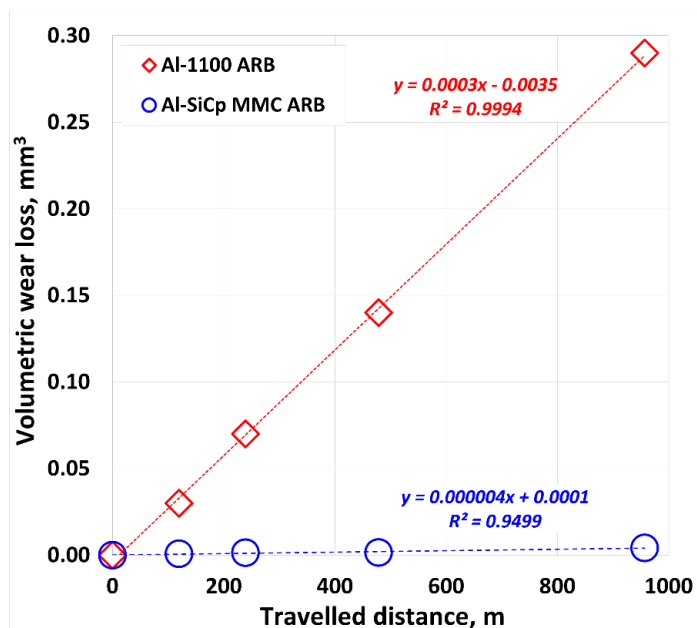


Figure 14. Wear resistance curves for the ARB laminates.

Figures 15(a,b) portrays OM views of worn surfaces of the materials tested, respectively Al-1100 ARB and Al-SiCp MMC ARB laminates.

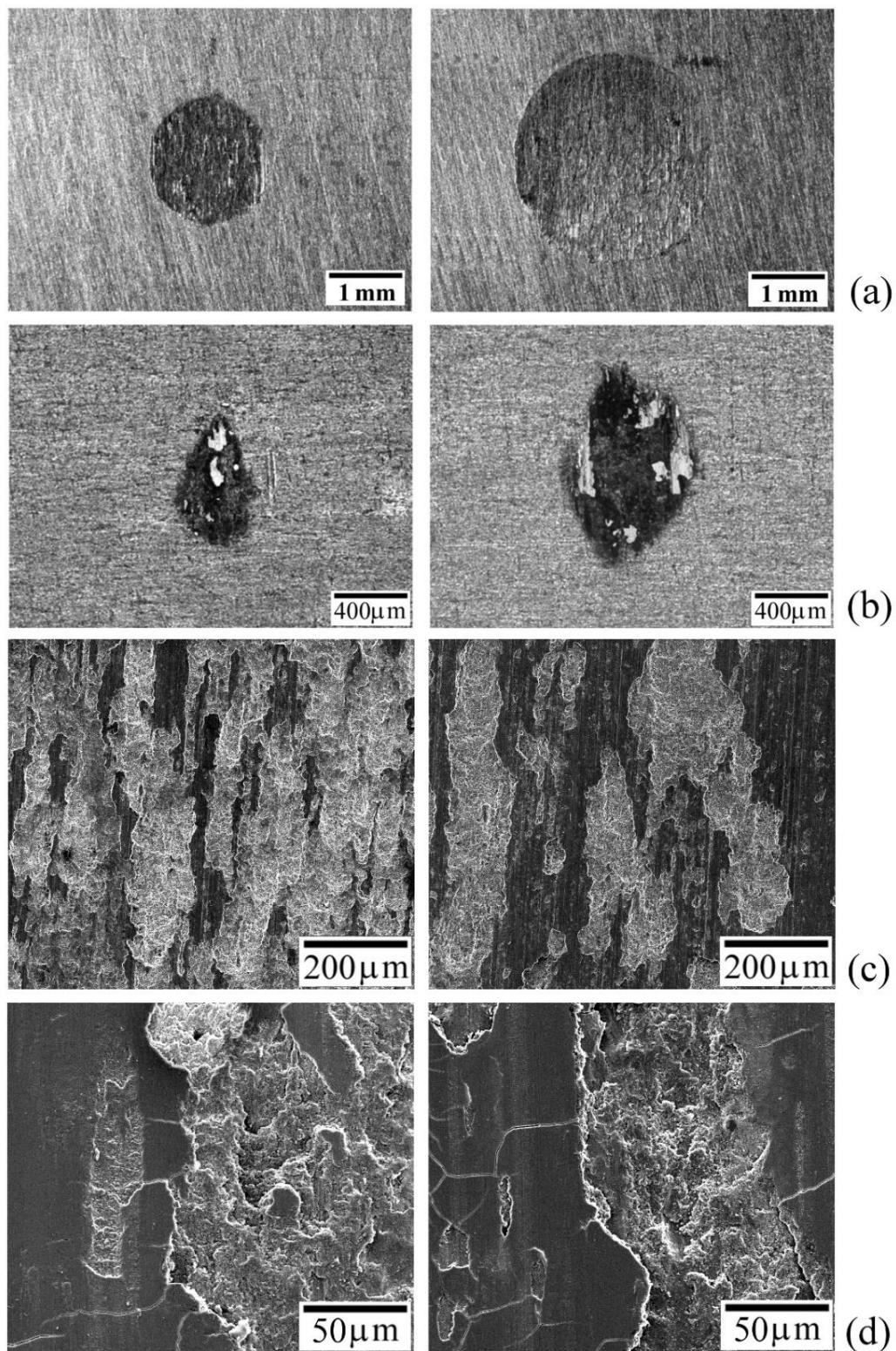


Figure 15. (a,b) OM fractographic views at two different wear test times, respectively 5 and 40 min, for respectively Al-1100 ARB and Al-SiCp MMC ARB laminates. (c,d) SEM fractographic views (SE mode) of Al-1100 ARB (left) and Al-SiCp MMC ARB (right).

From left to right, one can see the calottes formed at test times of, respectively, 5 and 40 min.

Figures 15(c,d) exhibits respective SEM views at two different magnitude of images. In Fig.15(c) two predominant wear mechanisms can be identified, namely, abrasion producing dark grooving marks, and delamination presenting bright alveolar aspect. In delamination, the material is worn in a layer-by-layer basis, while the material loss by abrasion occurs by friction mechanism, which is intensified by delamination.

Significantly more widespread wear damages are noticed for the Al-1100 ARB, thus confirming the plot provided in Fig.14. More detailed views in Fig.15(d) indicates the occurrence of large plastic deformation forming flat areas with gleamy aspect, especially in the MMC laminate. Its exceptional wear resistance may possibly result from the solid lubricant action of the ceramic particulate, which favours surface plastic strain at expenses of more deteriorating mechanisms like abrasion and delamination [16].

5. Conclusions

Micro-silicon carbide particles (SiCp at 5 vol.%) was incorporated to commercially pure aluminium 1100 by affordable accumulative roll bonding route. Microstructural changes and their effect on the mechanical properties and fracture mechanisms have been studied.

Main conclusions are as follows:

- i. Seven lamination passes reasonably dispersed SiCp in the aluminium matrix.

- ii. SiC imparted hardness, but only moderately enhanced tensile properties of unnotched and notched specimens.
- iii. Tensile properties of the metal matrix laminate were insensitive to geometrical stress raisers.
- iv. Ductile fracture mechanisms prevailed in tensile loading, while abrasion, adhesive and lamination mechanisms governed wear properties.
- v. SiCp granted outstanding wear resistance to the composite laminate by acting as efficient solid lubricant.
- vi. The inexpensive composite laminate can be a worthwhile option for applications where superior wear resistance and notch insensitivity offset some limitations on mechanical strength.

Acknowledgments: One of the authors (Pereira G.S.) acknowledges the National Council for Scientific and Technological Development (CNPq-Brazil) for scholarship (Process: 160283/2014-0). This study was partly financed by Coordination for Improvement of Higher Education Staff (CAPES-Brazil) through Financial Support Code 001.

CRedit author statement - Pereira G.S.: Conceptualization, Methodology, Validation, Investigation, Draft Writing and Review; Da Silva E.P.: Validation and Review; Requena G.C.: Validation and Review; Avila J.A.: Draft Writing and Review; Tarpani J.R.: Conceptualization, Methodology, Validation, Investigation, Draft Writing, Review and Editing, Visualization, Supervision.

Conflict of interest: The authors declare no conflict of interest.

References

- [1] Liu, Q.; Qi, F.; Wang, Q.; Ding, H.; Chu, K.; Liu, Y.; Li, C. The influence of particles size and its distribution on the degree of stress concentration in particulate reinforced metal matrix composites. *Materials Science & Engineering A*, **2018**, v.731,p.351-359. <https://doi:10.1016/j.msea.2018.06.067>
- [2] Khadir, A.I.; Fathy, A. Enhanced strength and ductility of Al-SiC nanocomposites synthesized by accumulative roll. *Journal of Materials Research and Technology*, **2019**, v.9, p.478-489. <https://doi.org/10.1016/j.jmrt.2019.10.077>
- [3] Garg, P.; Jamwal, A.; Kumar, D.; Sadasivuni K.K.; Hussain, C.M.; Gupta, P. Advance research progresses in aluminium matrix composites: manufacturing & applications. *Journal of Materials Research and Technology*, **2019**, v.9, p.4924-4939. <https://doi.org/10.1016/j.jmrt.2019.06.028>
- [4] Alizadeh, M.; Paydar, M.H. Fabrication of nanostructure Al/SiCP composite by accumulative roll-bonding (ARB) process. *Journal of Alloys and Compounds*, **2010**, v.492, p. 231-235. <https://doi.org/10.1016/j.jallcom.2009.12.026>
- [5] Alizadeh, M.; Paydar, M.H. Fabrication of Al/SiCP composite strips by repeated roll-bonding (RRB) process. *Journal of Alloys and Compounds*, **2009**, v.477, p.811-816. <https://doi.org/10.1016/j.jallcom.2008.10.151>
- [6] Saito, Y.; Tsuji, N.; Utsunomiya, H.; Sakai, T.; Hong, R.G. Ultra-fine grained bulk aluminum produced by accumulative roll-bonding (ARB) process. *Scripta Materialia*, **1998**, v.39, p.1221-1227. [https://doi.org/10.1016/S1359-6462\(98\)00302-9](https://doi.org/10.1016/S1359-6462(98)00302-9)
- [7] Saito, Y.; Utsunomiya, H.; Tsuji, N.; Sakai, T. Novel ultra-high straining process for bulk materials-development of the accumulative roll-bonding (ARB)

- process. *Acta Materialia*, **1999**, v.47, p.579-583. [https://doi.org/10.1016/S1359-6454\(98\)00365-6](https://doi.org/10.1016/S1359-6454(98)00365-6)
- [8] Ruppert, M.; Bohm, W.; Nguyen, H.; Hoppel, H.W.; Merklein, M.; Goken, M. Influence of upscaling accumulative roll bonding on the homogeneity and mechanical properties of AA1050A. *Journal of Materials Science*, **2013**, v.48, p.8377-8385. <https://doi.org/10.1007/s10853-013-7648-3>
- [9] Chen, M.; Hsieh, C.; Wu, W. Microstructural characterization of Al/Mg alloy interdiffusion mechanism during accumulative roll bonding. *Metals and Materials International*, **2007**, v.13, p.201-205. <https://doi.org/10.1007/BF03027805>
- [10] Li, B.L.; Tsuji, N.; Kamikawa, N. Microstructure homogeneity in various metallic materials heavily deformed by accumulative roll-bonding. *Materials Science and Engineering: A*, **2006**, v.423, p.331-342. <https://doi.org/10.1016/j.msea.2006.02.028>
- [11] Tsuji, N.; Saito, Y.; Lee, S.; Minamino, Y. ARB (accumulative roll-bonding) and other new techniques to produce bulk ultrafine grained materials. *Advanced Engineering Materials*, **2003**, v.5, p.338-344. <https://doi.org/10.1002/adem.200310077>
- [12] Jamaati, R.; Toroghinejad, M.R. Investigation of the parameters of the cold roll bonding (CRB) process. *Materials Science and Engineering: A*, **2010**, v.527, p.2320-2326. <https://doi.org/10.1016/j.msea.2009.11.069>
- [13] Amirkhanlou, S.; Rahimian, M.; Ketabchi, M.; Parvin, N.; Yaghinali, P.; Carreño, F. Strengthening mechanisms in nanostructured Al/SiCp composite manufactured by accumulative press bonding. *Metallurgical and Materials Transactions A*, **2016**, v.47, p.5136-5145. <https://doi.org/10.1007/s11661-016-3666-5>
- [14] Liu, C.Y.; Wang, Q.; Jia, Y.Z.; Zhang, B.; Jing, R.; Ma, M.Z.; Jing, Q.; Liu,

R.P. Evaluation of mechanical properties of 1060-Al reinforced with WC particles via warm accumulative roll bonding process. *Materials & Design*, **2013**, v.43, p.367-372.

<https://doi.org/10.1016/j.matdes.2012.07.019>

[15] Farhadipour, P.; Sedighi, M.; Vini, M.H. Using warm accumulative roll bonding method to produce Al-Al₂O₃ metal matrix composite. *Proceedings of the Institution of Mechanical Engineers, Part B: Journal of Engineering Manufacture*.

2017, v.231, p.889-896. <https://doi.org/10.1177/0954405417703421>

[16] Ghalehbandi, S.M.; Malaki, M.; Gupta, M. Accumulative roll bonding - a review. *Applied Sciences*, **2019**, v.9, p.3627-3659. <https://doi.org/10.3390/app9173627>

[17] Lee, S.H.; Kim, W.J.; Utsunomiya, H. Fabrication and evaluation of nanostructure Al-SiCp composite by accumulative roll-bonding. *Journal of Nanoscience and Nanotechnology*, **2011**, v.11, p.7451-7455.

<https://doi.org/10.1166/jnn.2011.4767>

[18] Alizadeh, M.; Paydar, M.H.; Terada, D., Tsuji, N. Effect of SiC particles on the microstructure evolution and mechanical properties of aluminum during ARB process. *Materials Science and Engineering: A*, **2012**, v.540, p.13-23.

<https://doi.org/10.1016/j.msea.2011.12.026>

[19] Jamaati, R.; Amirkhanlou, S.; Toroghinejad, M.R.; Niroumand, B. Effect of particle size on microstructure and mechanical properties of composites produced by ARB process. *Materials Science and Engineering: A*, **2012**, v.528, p.2143-2148.

<https://doi.org/10.1016/j.msea.2010.11.056>

[20] Wagih, A.; Fathy, A.; Ibrahim, D.; Elkady, O.; Hassan, M. Experimental investigation on strengthening mechanisms in Al-SiC nanocomposites and 3D FE simulation of Vickers indentation. *Journal of Alloys and Compounds*, **2018**, v.752,

p.137-147. <https://doi.org/10.1016/j.jallcom.2018.04.167>

[21] Melaibari, A.; Fathy, A.; Mansouri, M.; Eltaher, M.A. Experimental and numerical investigation on strengthening mechanisms of nanostructured Al-SiC composites. *Journal of Alloys and Compounds*, **2019**, v.774, p.1123-1132.

<https://doi.org/10.1016/j.jallcom.2018.10.007>

[22] Fathy, A.; Ibrahim, D.; Elkady, O. Hassan, M. Evaluation of mechanical properties of 1050-Al reinforced with SiC particles via accumulative roll bonding process. *Journal of Composite Materials*, **2019**, v.53, p.209-218.

<https://doi.org/10.1177/0021998318781462>

[23] Darmiani E.; Danaee I.; Golozar M.A.; Toroghinejad M.R.; Ashrafi A.; Ahmadi A. Reciprocating wear resistance of Al-SiC nano-composite fabricated by accumulative roll bonding process. *Materials & Design*, **2013**, v.50, p.497-502.

<https://doi.org/10.1016/j.matdes.2013.03.047>

[24] Amirkhanlou S.; Jamaati R.; Niroumand B.; Toroghinejad M.R. Fabrication and characterization of Al/SiCp composites by CAR process. *Materials Science and Engineering A*, **2011**, v.528, p.4462-4467. <https://doi.org/10.1016/j.msea.2011.02.037>

[25] Gee, M.; Gant, A.J.; Hutchings, I.M.; Kusano, Y.; Schiffman, K.; Van Acker, K.; Poulat, S.; Plint, G. Results from an interlaboratory exercise to validate the micro-scale abrasion test. *Wear*, **2005**, v.259, p.27-35.

<https://doi.org/10.1016/j.wear.2005.02.092>

[26] Santos Filho, O.C. Microestrutural and mechanical properties characterization of AA1100 and AA5052 alloys processed by accumulated roll bonding - ARB. Master's Dissertation. Politechnic School of Metallurgy and Materials Engineering.

<http://dx.doi.org/10.11606/D.3.2009.tde-29062009-103030>

- [27] Kaneko, S.; Fukuda, K.; Utsunomiya, H.; Sakai, T.; Saito, Y.; Furushiro, N. Ultra Grain refinement of aluminium 1100 by ARB with cross rolling. *Materials Science Forum*, **2003**, v.426, p.2649-2654.
<https://doi.org/10.4028/www.scientific.net/MSF.426-432.2649>
- [28] Kwan, C.; Wang, Z.; Kang, S.B. Mechanical behavior and microstructural evolution upon annealing of the accumulative roll-bonding (ARB) processed Al alloy 1100. *Materials Science and Engineering: A*, **2008**, v.480, p.148-159.
<https://doi.org/10.1016/j.msea.2007.07.022>
- [29] Bagherpour, E.; Reihanian, M.; Miyamoto, H. Tailoring particle distribution Non-uniformity and grain refinement in nanostructured metal matrix composites fabricated by severe plastic deformation (SPD): a correlation with flow stress. *Journal of Materials Science*, **2017**, v.52, p.3436–3446. <https://doi.org/10.1007/s10853-016-0632-y>
- [30] Khadir, A.I.; Fathy, A. Enhanced strength and ductility of Al-SiC nanocomposites Synthesized by accumulative roll bonding. *Journal of Materials Research and Technology*, **2019**, 12p. <https://doi.org/10.1016/j.jmrt.2019.10.077>
- [31] Meselhy, A.F.; Reda, M.M. Investigation of mechanical properties of nanostructured Al-SiC composite manufactured by accumulative roll bonding. *Journal of Composite Materials*, **2019**, v.53, p.3951–3961.
<https://doi.org/10.1177/0021998319851831>
- [32] Oliveira, J.D.C.P.T.; Padilha, A.F. Microstructural characterization of AA1100, AA1050 and AA1070 commercial aluminums and AA1199 super pure aluminum. *Rem: Revista Escola de Minas*, **2009**, v.62, p.373-378.
<http://dx.doi.org/10.1590/S0370-44672009000300017>

- [33] Adam, K.; Zöllner, D.; Field, D.P. 3D microstructural evolution of primary recrystallization and grain growth in cold rolled single-phase aluminum alloy. *Modelling and Simulation in Materials Science and Engineering*, **2018**, v.26, 16p. <https://doi.org/10.1088/1361-651X/aaa146>
- [34] Kondo, S.; Mitsuma, T.; Shibata, N.; Ikuhara, Y. Direct observation of individual dislocation interaction processes with grain boundaries. *Science Advances*, **2016**, v.2, 11p. <https://doi.org/10.1126/sciadv.1501926>
- [35] Shamanian, M.; Mohammadnezhad, M.; Asgari, H.; Szpunar, J. Fabrication and characterization of Al-Al₂O₃-ZrC composite produced by accumulative roll bonding (ARB) process, *Journal of Alloys and Compounds*, **2015**, v.618, p.19-26. <https://doi.org/10.1016/j.jallcom.2014.08.136>
- [36] Heydari V.M.; Farhadipour, P. Fabrication of AA1060/Al₂O₃ composites by warm accumulative roll bonding process and investigation of its mechanical properties and microstructural evolution. *International Journal of Advanced Design and Manufacturing Technology*, **2017**, v.10, p.91-98. <https://www.magiran.com/paper/1781372>
- [37] Yousefian, R.; Emadoddin, E.; Baharnezhad, S. Manufacturing of the aluminum metal-matrix composite reinforced with micro-and nanoparticles of TiO₂ through accumulative roll bonding process (ARB). *Reviews on Advanced Materials Science*, **2018**, v.55; p.1-11. <https://doi.org/10.1515/rams-2018-0022>
- [38] Cepeda-Jiménez, C., Pozuelo, M., García-Infanta, J. Interface effects on the fracture mechanism of a high-toughness aluminum-composite laminate. *Metallurgical and Materials Transactions A*, **2009**, v.40 p.69-79. <https://doi.org/10.1007/s11661-008-9679-y>

- [39] Chen, Z.; Chen, Q. Interface shear actions and mechanical properties of nanostructured dissimilar Al alloy laminated metal composites. *Journal of Nanomaterials*, **2015**, v.2015, 14p. <http://dx.doi.org/10.1155/2015/612029>
- [40] Huang, C.X.; Wang, Y.F.; Ma, X.L.; Yin, S.; Höppel, H.W.; Göken, M.; Wu, X.L.; Gao, H.J.; Zhu, Y.T. Interface affected zone for optimal strength and ductility in heterogeneous laminate. *Materials Today*, **2018**, v.21, p.713-719. <https://doi.org/10.1016/j.mattod.2018.03.006>
- [41] Sobie, C.; McPhie, M.G.; Capolungo, L.; Cherkaoui, M. The effect of interfaces on the mechanical behaviour of multilayered metallic laminates. *Modelling and simulation in materials science and engineering*, **2014**, v.22, 14p. <https://doi.org/10.1088/0965-0393/22/4/045007>
- [42] Qu, R.; Zhang, P.; Zhang, Z. Notch effect of materials: strengthening or weakening? *Journal of Materials Science & Technology*, **2014**, v.30, p.599-608. <https://doi.org/10.1016/j.jmst.2014.04.014>
- [43] Shin, S.; Cho, S.; Lee, D.; Kim, Y.; Lee, S.B.; Lee, S.K.; Jo, I. Microstructural evolution and strengthening mechanism of SiC/Al composites fabricated by a liquid-pressing process and heat treatment. *Materials*, **2019**, v.12, p.3374-3384. <https://doi.org/10.3390/ma12203374>
- [44] Min, S.O.N.G. Effects of volume fraction of SiC particles on mechanical properties of SiC/Al composites. *Transactions of Nonferrous Metals Society of China*, **2009**, v.19, 1400-1404. [https://doi.org/10.1016/S1003-6326\(09\)60040-6](https://doi.org/10.1016/S1003-6326(09)60040-6)
- [45] Liu, C.Y.; Jiang, H.J.; Wang, C.X.; Li, Y.P.; Luo, K. Fabrication and strengthening mechanisms of Al/WC particles composite prepared by accumulative roll

bonding. *Materials Science Forum*, **2016**, v.849, p.397-401.

<https://doi.org/10.4028/www.scientific.net/msf.849.397>